Understanding Adsorption-Desorption Dynamics of BMP-2 on Hydroxyapatite (001) Surface

Xiuli Dong, Qi Wang, Tao Wu, and Haihua Pan
Department of Chemistry, Zhejiang University, Hangzhou, China

ABSTRACT The interaction between protein molecules and the hydroxyapatite (HAP) crystal is an important research topic in many fields. However, the nature of their noncovalent bonding is still not clear at the atomic level. In this work, molecular dynamics simulation, steered molecular dynamics simulation, and quantum chemistry calculations were used to study the adsorption-desorption dynamics of BMP-2 on HAP (001) surface. The results suggest that there are three types of functional groups through which BMP-2 can interact with HAP crystallite, and they are –OH, $–NH_2$, and $–COO^-$. Based on the different orientations of protein, each might interact with HAP crystallite individually, or, two or three of them can work cooperatively. Concerning the mechanisms of interaction, it is found that the water-bridged H-bond plays an important role, which is the main force for groups without net charges. If there were more than one set of adsorption groups for a certain orientation of protein, the adsorption-desorption process would likely be stepwise. On the contrary, if there were only one set, there would be only the key-adsorption period. The results of density functional theory calculations confirm the actual existence of this type of water-bridged H-bond. Furthermore, it is also found that the CHARMM27 force field could provide correct structural information qualitatively, although the data are slightly different from those obtained by UB3LYP/6-31G* method.

INTRODUCTION

The phenomenon of protein adsorption on inorganic materials is one of the most interesting topics in a wide variety of fields, such as biophysics, biochemistry, biomaterials, biomineralization, and clinical medical devices (1–3). It is especially important to cellular response studies (4,5). Hydroxyapatite [HAP, $Ca_{10}(PO_4)_6(OH)_2$] is the major inorganic component of bones and teeth. In the last decade, it has received much attention in materials science and medical fields (6,7). In particular, it has tissue-engineering applications where HAP scaffolds are often used due to their biocompatibility and in orthopedic applications where implants are coated with HAP to ensure better bonding. Furthermore, HAP exhibits large osteoconductive properties in vivo (8) and is considered as a model matrix to investigate fundamental mechanisms of biomineralization and bone formation (9). In brief, all these applications are related with its special interaction with biological molecules, which mainly are proteins. In fact it has already been found that there are many factors influencing the interaction between proteins and the HAP surface (10,11), such as protein structures, special texture of HAP surfaces, surroundings, and so on. With the influence of these factors, the interaction mechanisms for different proteins might be various. There have been many theoretical and experimental studies on this subject. For example, some researchers reported that the strong adsorption of some proteins with HAP was mediated by the acidic N-terminal (12,13). As to the interaction mechanism, it was proven that the electrostatic interaction between HAP and protein molecules was the dominating factor (14,15). In addition, atomic-force microscopy experiments (16,17) illustrated that the difference of adsorption was probably caused by protein structure characteristics. These studies greatly extended our knowledge of the dynamic behaviors of proteins on the HAP surface. However, they could not provide enough microscopic details for the molecular interactions. Therefore, it is necessary to investigate the interaction between proteins and HAP thoroughly, and to provide a better understanding at the atomic level.

Molecular dynamics (MD) simulation provides a powerful semitheoretical tool at the atomic level, and it has been extensively applied to biomolecular systems (18). Specifically, it is acceptable to achieve equilibrium conformations (3,19,20). However, concerning relatively large conformational changes in molecules on large timescales, such as the adsorption-desorption process of proteins on the HAP surface, the CPU time of MD simulation is too long to be computationally accepted. Here, the steered molecular dynamics (SMD) simulation would be a good alternative. SMD, developed by Schulten and co-workers (21,22), is another effective way to explore biological processes (23,24). It shortens the simulation time for an interesting process greatly through disturbances. In addition, it reveals the details of molecular interactions well, thereby providing important information about the molecular mechanisms underlying these processes. These two methods have been applied in our group successfully (3).

Bone morphogenetic proteins (BMPs) are one of the three growth factor systems involved in bone formation. They are incorporated into mineralized bone matrix and retain activity when extracted from bones. They regulate a diverse array of cellular functions during development and adult stages (25) of the human body. Studies on BMPs would be helpful to the understanding of bone formation, fracture healing, and bone

Submitted December 16, 2006, and accepted for publication March 29, 2007.
Address reprint requests to T. Wu, E-mail: tao_wu@zju.edu.cn.
Editor: Klaus Schulten.
© 2007 by the Biophysical Society
0006-3495/07/08/750/10 $2.00
doi: 10.1529/biophysj.106.103168

growth around implants. BMPs are also of considerable interest currently as therapeutic agents for healing fractures and periodontal bone defects. Combinations of BMPs and HAP are expected to provide potent alternatives for the autogeneration of bone grafts. However, there are only a few detailed mechanism studies about HAP-BMPs combinations. Many of the studies performed so far are in vivo experiments (26–28), and lack atomic-level detail. This is an essential problem, and very important to these specific applications. Therefore, in this work, we selected BMP-2 as an example and employed atomistic simulation methods to investigate the dynamic behaviors of BMPs on the HAP surface. As to the HAP crystallite, the (001) face is one of the extensively studied surfaces both experimentally and computationally (29,30). As suggested by many experiments, HAP is prone to elongate in the direction of the c axis during its growth (31). Thus, both MD and SMD simulations were conducted on the HAP (001) surface in the c axis (the z axis in the Cartesian coordinates) direction.

MATERIALS AND METHODS

The starting structure of BMP-2 was downloaded from the Brookhaven Protein DataBank (http://www.rcsb.org/pdb/explore/explore.do?structureId=3BMP). HAP is in the space group of $P6_3/m$ and its unit cell parameters are $a = b = 0.943$ nm and $c = 0.688$ nm (32).

Firstly, the BMP-2 downloaded was solvated in a water box. Considering that the BMP-2 carries two negative charges, two Na^+ ions were added as counterions to neutralize the solvated system. These two Na^+ ions also made the system a more typical biological environment. A standard MD procedure of 1 ns was run to equilibrate the geometry structure of BMP-2. Then, a system including the equilibrated BMP-2 molecule (1641 atoms), HAP crystallite (16,940 atoms), and two Na^+ counterions was built. To resemble the aqueous environment more closely, the whole system was completely solvated in a periodic water box of $66.0 \times 40.8 \times 170.0$ Å^3 (7836 water molecules). Then, a 2-ns MD run was carried out to equilibrate this new system using NAMD (33) software with CHARMM27 force field (34). The parameters for HAP were taken from the work of Hauptmann et al. (35), an accepted description of the structure and the nature of HAP at different temperatures. The parameters for the cross interactions came from the Lorentz-Berthelot mixing rule (36),

$$\sigma_{ij} = \frac{(\sigma_{ii} + \sigma_{jj})}{2}, \quad (1)$$

$$\varepsilon_{ij} = \sqrt{\varepsilon_{ii}\varepsilon_{jj}}. \quad (2)$$

This rule was extensively used to calculate the intermolecular potential between pairs of nonidentical atoms in biomaterial fields (37–39). Here, we used SPC water model (40) to explicitly simulate the solvent. The particle-mesh Ewald method (41) was employed to calculate the long-range electrostatic interactions, with a value of 13.5 Å for the separation of the direct and reciprocal space summations. The van der Waals interactions were truncated at 12 Å (cutoff). All atoms in this system, including all hydrogen atoms and water molecules, were modeled explicitly. A time step of 2 fs was used with atom coordinates saved every 1 ps. During the MD equilibration simulation, the Langevin thermostat method was applied to control the constant temperature of 310 K and the constant pressure of 101.3 kPa.

Based on the equilibration structure after 2-ns MD simulation and the parameters, SMD simulations of constant velocity pulling were carried out. Here, the HAP crystallite was fixed and the external forces were applied uniformly on BMP-2 to pull its backbone atoms along the c axis. In the constant velocity pulling simulation, the SMD atom is attached to a dummy atom via a virtual spring. This dummy atom is moved at a constant velocity and then the force between them is measured (33).

Through the MD and SMD simulations, it is found that the water-bridged H-bond is the main attractive force contributing to the interaction between HAP and the residues with no net charges. Considering that the structure parameters obtained through molecular mechanics methods are not very precise, a series of density functional theory (DFT) calculations were performed in the LDA and UB3LYP/ 6-31G* level of theory, with Materials Studio (42,43) and Gaussian 03 (44) packages, respectively. These two methods have been extensively used in similar systems (45–48). To facilitate these calculations and to maintain the structure of the HAP crystallite, only the structures involved in the water-bridged H-bond were optimized. The other portion of BMP-2, which does not belong to the given interactive residues, was replaced by a $-CH_3$ group. Since the aqueous environment of proteins is very important for their physical and chemical properties, the Onsager reaction field approach was used, and the solvent employed was water with a dielectric constant of 78.39.

RESULTS AND DISCUSSION

Equilibrium conformation by MD simulation

A MD simulation is essential to achieve equilibrium states for biological molecular systems. In this work, two criterions have been adopted to judge whether the system achieved equilibrium or not, namely, the potential energy of protein (41,42) and the root mean-square deviation (RMSD) (25) of the backbone atoms (without hydrogen) of BMP-2. To describe the system more exactly, the potential energy of BMP-2 was extracted separately (see Fig. 1). Since too much information has been obtained through the 2-ns MD equilibration simulation, for clarity only the curves of the last 0.5 ns were illustrated. During the 2-ns MD simulation at 310 K, the whole structure remained basically stable. As shown in Fig. 1, the potential energy of BMP-2 keeps fluctuating slightly around the energy of 550 kcal mol^{-1} during the last 0.5 ns, indicating that the system has achieved the equilibrium state. As to the curve of RMSD, it also suggests that the system is stable, because the curve changes mildly and fluctuates in a narrow range (~0.5 Å) during the last 0.5 ns of MD simulation. Fig. 2 *a* illustrates the equilibrium structure of BMP-2 and HAP system.

Adsorption-desorption mechanism by SMD simulation

Based on the equilibrium structure, a SMD simulation of 1 ns was conducted. The virtual spring between the dummy atoms and the SMD atoms had a spring constant of 20 kcal mol^{-1} Å^{-2} and the constant velocity was 0.042 Å ps^{-1}. All the analysis below is based on this simulation.

The snapshots of this system during the whole 1 ns SMD simulation are presented in Fig. 2. Analyzing the trajectories obtained, it can be observed how the process from adsorption to desorption is stepwise. At the initial stage (0 ps), there was no adsorbed residue on the interface of BMP-2 (Fig. 2 *a*), so when an external force is applied, the protein began to leave

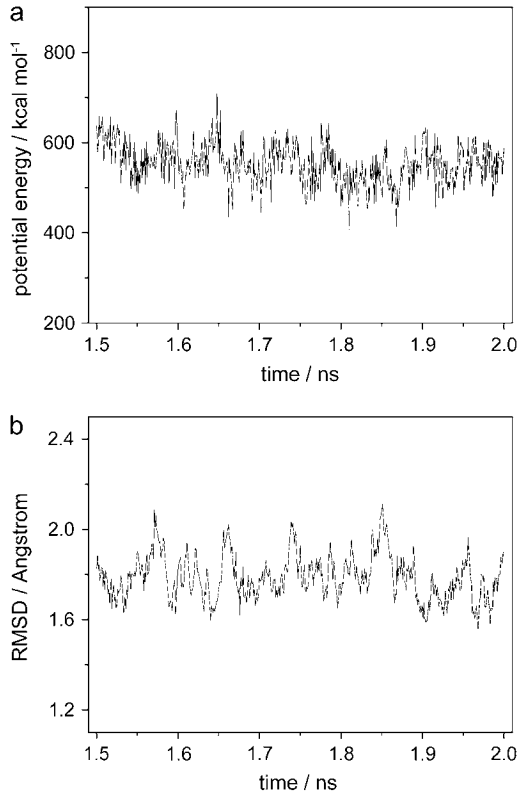

FIGURE 1 (*a*) Potential energy, and (*b*) RMSD of BMP-2 versus simulation time.

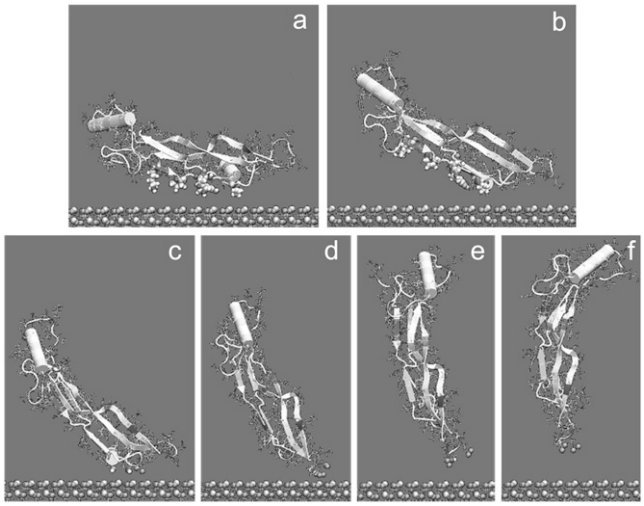

FIGURE 2 Snapshots of 1-ns SMD simulation with key residues or atoms marked (all the water molecules are omitted for clarity, and O, N and H atoms are marked *light shaded*, *dark shaded*, and *open*, respectively). (*a*) 0 ps; (*b*) 100 ps; (*c*) 200 ps; (*d*) 400 ps; (*e*) 600 ps; and (*f*) 700 ps. The marked residues (from *left* to *right*) are: (*a*,*b*) Lys^{15}, Pro^{18}, His^{39}, Tyr^{20}, and Pro^{36}; (*c*) Ser^{24}, Asn^{29}, and Asp^{30}; and (*d–f*) Glu^{96}, Asn^{95}, and Glu^{94}.

the HAP surface immediately (Fig. 2 *b*). This is the nonadsorption period. Although there were some residues closer to HAP (001) surface, they were not adsorbed. We defined these residues as nonadsorption residues. As the simulation proceeded, the residues of BMP-2 kept vibrating to reach the best interaction with HAP under the influence of external force and thousands of surrounding water molecules. Slowly, some residues were exposed to the HAP (001) surface from the main body of BMP-2, and became adsorbed on the surface (Fig. 2 *c*). Considering that these first adsorbed residues are located in the middle part of the BMP-2 (at the equilibrium position) and that there were already residues that interacted strongly with the HAP (001) surface in the right-hand part of BMP-2, we consider that these adsorbed residues played the role of the fulcrum in a lever. These were thus labeled as the fulcrum-adsorption residues and the time gap is called fulcrum adsorption period, hereinafter. Under the external force, which was applied equally to the backbone atoms of BMP-2, the left-hand part of BMP-2 began to turn up. According to the lever principle, the right-hand part was much closer to the HAP surface (Fig. 2, *c–e*). This change again promoted the interaction between the right adsorption residues and HAP. This is the key-adsorption period. Our further analysis proved that the adsorption of these key residues was much stronger and lasted for a longer time than the fulcrum-adsorption (Figs. 4 and 6). Thus, the adsorption of these residues was a main interaction force and we defined them as key-adsorption residues (Fig. 2, *d–f*). At 600 ps, the interaction between the key-adsorption residues and the HAP surface was broken under the external force and BMP-2 began to be desorbed form HAP crystallite. From then on, no other adsorption phenomenon occurred. At 700 ps, the desorption process was completely finished and the orientation of BMP-2 did not change any more (Fig. 2 *f*). It maintained a perpendicular orientation with respect to the HAP (001) surface and moved away from HAP until the end of SMD simulation (1000 ps). Therefore, it seems that the right-hand part would be the most prone to be adsorbed on the HAP (001) surface. In addition, it is worthwhile to note that the positions of the fulcrum-adsorption and key-adsorption functional groups are on different parts of BMP-2, which is different from the theoretical and experimental results found for the other proteins (3,13). This indicates that the type of interaction varies for different structure characteristics of proteins, as experimental results suggested by Wallwork et al. (16).

As shown in Fig. 2, BMP-2 is actually interacting end-on rather than face-on. It is interesting to explore the reasons behind this phenomenon. The SMD details reveal that it is the lever principle that results in the dramatic rotation phenomenon. As mentioned above, there is no interaction between the left-hand part of BMP-2 and HAP, but there is for the middle and right-hand part. Apparently, the force applied on BMP-2 is not balanced. According to the lever principle, the BMP-2 will rotate and the attractive force on the middle part of BMP-2 acts as the fulcrum. Along with the

rotation, the key-adsorption groups at right part are pulled much closer to the HAP surface. Correspondingly, the strong interaction accelerates the rotation process until the BMP-2 ends up completely.

The nonadsorption period

As shown in Fig. 2 *a*, there were five nonadsorption residues at the initial configuration (at 0 ps), which were Lys^{15}, Pro^{18}, His^{39}, Tyr^{20}, and Pro^{36}. The relative displacements between these residues and HAP surface along the *z* axis (the *c* axis of HAP crystallite) are shown in Fig. 3. From observation of the figure, it is found that the displacements are almost linear with the SMD time, implying that this process is velocity-invariable for these residues. This is consistent with the prearranged SMD simulation condition. If there were any interaction between these residues and HAP crystallite, it would resist the external force applied and would make these residues stay for a relatively long time. This phenomenon was not observed and one could thus conclude that there is hardly any interaction between these residues and HAP (001) surface. If one scrutinizes the structures of these five residues, it is evident that none of them have strongly electron-attracting groups except for the –COOH group, which forms a peptide bond with another residue. Therefore, no significant adsorption phenomenon is to be expected even if they were close to the HAP crystallite in the initial state. Of course, there should be hydrogen bonds (H-bonds) between the strongly electronegative O or N atoms and the surrounding H_2O molecules, but this type of H-bond is present everywhere and does not contribute to the interaction or adsorption between these nonadsorption residues and HAP crystallite.

The fulcrum-adsorption period

As the SMD simulation proceeded, the fulcrum-adsorption residues, Ser^{24}, Asn^{29}, and Asp^{30} in the middle part of BMP-2, began to stick out and the first adsorption phenomenon was detected (Fig. 2 *c*). The displacement changes of these three residues versus the SMD simulation time are shown in Fig. 4. In the figure, one can see how the displacement of Asp^{30} decreases dramatically from 16.3 Å (0 ps) to 4.6 Å (165 ps), and then it remains ~5 Å for ~200 ps. This is the direct evidence that Asp^{30} forms a relatively strong interaction with the HAP (001) surface and then it is adsorbed. From 384 ps onwards, the displacement increased rapidly and these residues began to be desorbed until the end of SMD simulation (1000 ps) with a displacement of 39.3 Å. This whole curve suggested that the time of 1 ns was long enough to simulate

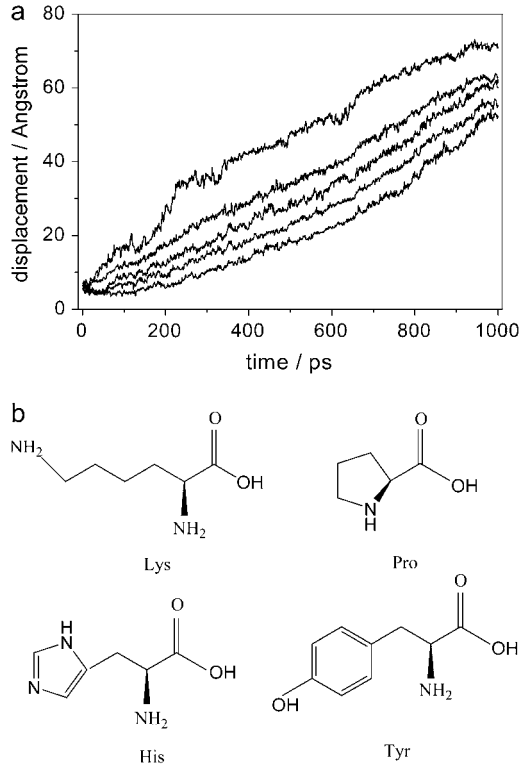

FIGURE 3 (*a*) Displacement between the nonadsorption residues (*from top to bottom*, Lys^{15}, Pro^{18}, His^{39}, Tyr^{20}, and Pro^{36}) and the HAP (001) surface in the *z* axis versus SMD time, and (*b*) the structures of the nonadsorption residues.

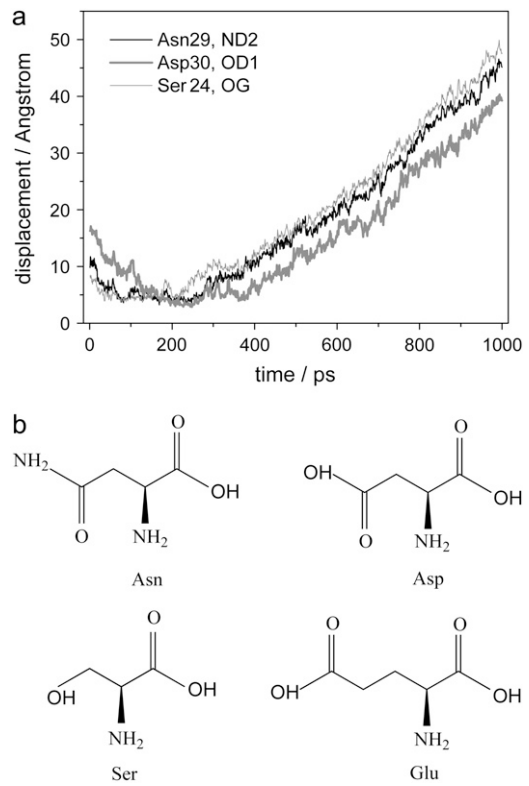

FIGURE 4 (*a*) Displacements between the fulcrum-adsorption residues and the HAP (001) surface in the *z* axis versus SMD time, and (*b*) the structures of the adsorption residues.

the integrated adsorption-desorption process of BMP-2 on HAP (001) surface. This behavior was also observed for the other two fulcrum-adsorption residues and the two key-adsorption residues (Figs. 4 and 6). As to Asn^{29} and Ser^{24}, their adsorptions spent ~270 ps and 220 ps, respectively.

The question is how these three residues interact with the HAP (001) surface. After a careful analysis of the movement of BMP-2 step by step for 1 ns, it was found that the key point is the formation of water-bridged H-bonds (Fig. 5). Firstly, the adsorption residues form H-bonds with the closest water molecules around them. Then this bonded H_2O interacts with another water molecule through intermolecular H-bond. Finally, the second H_2O molecule forms an H-bond with the O atom of the first layer PO_4^{3-} in HAP. During the entire SMD process, this type of water-bridged H-bond kept on forming and breaking. It was also found that the number of bridged water molecules was two at most. This number is in agreement with the distance of ~5 Å between the marked atoms and HAP surface. At 0 ps, the displacement of Ser^{24} was the smallest (~8 Å) among these three residues, so it interacted with HAP surface firstly through the water-bridged H-bond (Fig. 5 *a*). Then was Asn^{29}, which was ~10 Å away from HAP surface at the initial state. Through the strong proton donor (H atom), it was feasible to form H-bond and thus to interact with HAP surface (Fig. 5 *b*). While for Asp^{30}, the displacement at 0 ps was much farther than Ser^{24} and Asn^{29}, so it took another ~150 ps to be adsorbed onto HAP (Fig. 4). Correspondingly, it began desorbing slowly until 400 ps. It is worthwhile noting that $-COO^-$ is the active part of Asp^{30} and it is negative-charged. Considering that the outmost layer of HAP (001) surface is Ca^{2+} (see Fig. 2, where the *large open sphere* represents Ca^{2+} and the *small shaded sphere* represents the O atom of PO_4^{3-}), the existence of a Coulombic force is obvious, as reported by our simulation (3) and NMR experiments (14,15). At the same time, the $-COO^-$ has two electronegative O atoms, so there are water-bridged H-bonds as well. Under the cooperation of Coulombic force and water-bridged H-bonds, the Asp^{30} residue is the one with a closest distance to HAP. At 248 ps, the displacement was only 2.9 Å (Fig. 4). The VMD animation of this SMD process also showed that the water-bridged H-bonds are present not only between adsorption groups and HAP (Fig. 5, *a–c*), but also between one adsorption group and another (Fig. 5, *d–f*). Thus the adsorption and desorption curves for different residues mingled within a definite SMD time (Fig. 4). At the beginning, the $-NH_2$ of Asn^{29} and –OH of Ser^{24} interacted, which resulted in the superposition of the two curves for 50–200 ps. Then the Ser^{24} was pulled away, while Asp^{30} moved closer to HAP. Thus, Asn^{29} formed water-bridged H-bonds with Asp^{30} for the later time of 200–300 ps. In brief, the adsorption of fulcrum-adsorption residues on the HAP (001) surface is the result of the cooperative interaction of Coulombic force and water-bridged H-bonds, and the latter was the main adsorption mechanism for the residues without net charges.

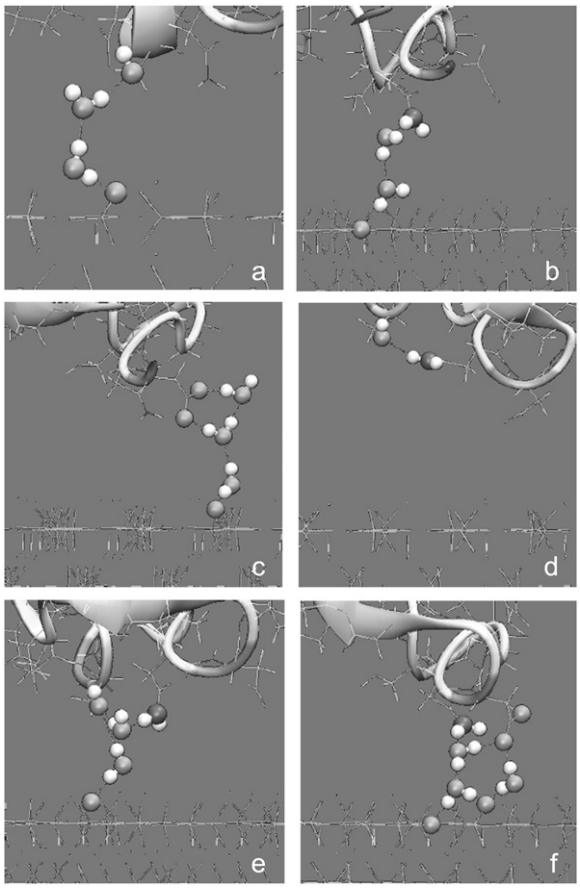

FIGURE 5 Snapshots of water-bridged H-bonds for the fulcrum-adsorption residues. (*a*) Ser^{24}-HAP; (*b*) Asn^{29}-HAP; (*c*) Asp^{30}-HAP; (*d*) Asn^{29}-Ser^{24}; (*e*) Asn^{29}-Ser^{24}; and (*f*) Asp^{30}-Asn^{29}. (Atoms: O, *light shaded*; N, *dark shaded*; H, *open*.)

However, the reason why the $-NH_2$ and –OH in the nonadsorption residues did not form this type of water-bridged H-bond remains unknown. The reason might come from the different structures of their neighboring part (Figs. 3 and 4). If the $-NH_2$ or –OH were bound to strongly electron-attracting groups directly, they would probably form water-bridged H-bonds. Otherwise, as in the case of the $-NH_2$ or –OH in the nonadsorption residues, which are bound to saturated alkyl chains or stable five- or six-numbered cycles, the relatively stable electron surroundings result in the considerable stability of $-NH_2$ or –OH in Lys^{15}, Pro^{18}, His^{39}, Tyr^{20}, and Pro^{36}. On the contrary, when they are present in the fulcrum-adsorption residues, the strongly electron-attracting effect of –C=O group changes their electron distribution and makes the electron cloud of O or N and H atoms overlapped much less. Therefore, it is more favorable to form H-bond with water molecules. Although the –OH in Ser^{24} does not bond with –C=O directly, it is very close to the peptide bond, and the effect is similar, therefore, the –OH in Ser^{24} also formed water-bridged H-bond with $PO4^{3-}$.

It should also be considered that there is a syntonic equilibrium as Eq. 3 (see below) for the structure mentioned above.

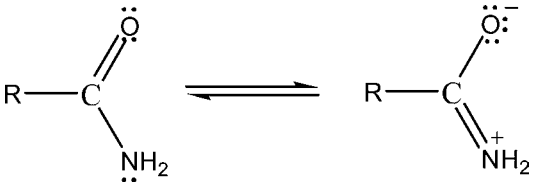

(3)

There are charged groups of $-O^-$ and $=NH_2^+$ in the right-hand structure, so there should be Coulombic force between Asn^{29} and HAP (001) surface. Namely, the Coulombic force should attribute to the adsorption between Asn^{29} and HAP to some extent. However, in general, the probability of the right-hand syntonic structure is small. Therefore, its influence on the adsorption would be little. That is to say, it is the water-bridged H-bond that plays the critical functional role for the adsorption between Asn^{29} and HAP (001) surface.

The key-adsorption period

As the SMD simulation time reaches 400 ps, the key-adsorption residues played critical functional roles. Actually, at ~230 ps, some adsorptions can be observed between Asn^{95}, Glu^{96}, and HAP (001) surface, i.e., both the fulcrum-adsorption residues and the key-adsorption ones contributed to the adsorption of BMP-2 onto HAP during the time gap between 200 and 400 ps. The difference is that the key-adsorption phase lasts for a much longer adsorption time, up to 350 ps (Fig. 6). Concerning the displacement of the different functional groups from HAP, Glu^{96} changed from ~17 Å in the initial state to ~3 Å in the adsorption state, and for Asn^{95}, the change was from ~23 Å to ~3 Å. Once both residues are at this distance, they remain there until the SMD time reaches ~600 ps. Both the dramatic displacement changes and the long time during which both residues stay at ~3 Å during the SMD implied the strong interaction between these two key-adsorption residues and the HAP (001) surface. Considering that the external force kept pulling BMP-2 away from the HAP crystallite, Asn^{95} and Glu^{96} began to be desorbed along with the motion of the whole protein from 600 ps. Once the strong interaction was broken, the displacement increased quickly and kept at almost a constant velocity just as we pre-set. This issue indicated that the desorption phenomenon has occurred. No other adsorption sites occurred for later simulation times. The orientation of BMP-2 changed very little within the pre-arranged periodic boundary conditions.

We thus found it is necessary to explore the interaction mechanism resulting in the adsorption and desorption phenomena between BMP-2 and HAP (001) surface in this period. The SMD simulation results suggested that the water-bridged H-bond plays the key role, just as the mechanism in the period of fulcrum-adsorption. The Asn^{95} residue is the same type of residue as Asn^{29}, which was active in the fulcrum adsorption period. So the mechanism of interaction can be assumed to be the same as in that case. That is to say, the main force is the water-bridged H-bond between the $-NH_2$ in Asn^{95} and the O atom in PO_4^{3-}. The corresponding

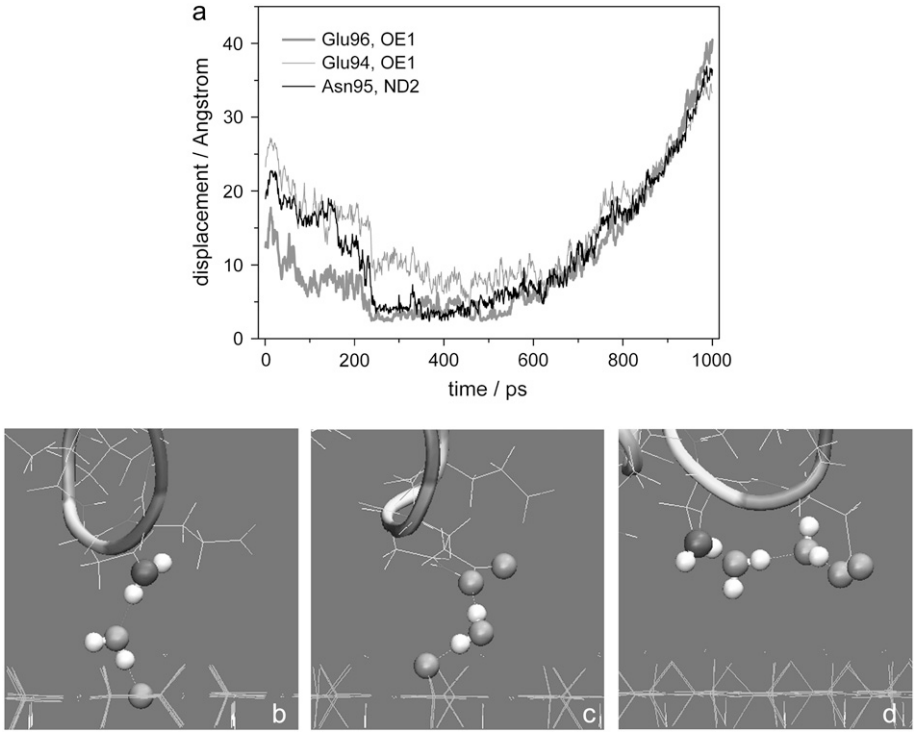

FIGURE 6 (*a*) Displacements between the key-adsorption residues and the HAP (001) surface in the *z* axis versus SMD time, and the snapshots of water-bridged H-bonds for different residues, (*b*) Asn^{95}-HAP, (*c*) Glu^{96}-HAP, and (*d*) Glu^{96}-Asn^{95}. (Atoms: O, *light shaded*; N, *dark shaded*; H, *open*.)

snapshot is shown in Fig. 6 *b*. Similarly, there might be Coulombic force considering the syntonic equilibrium (Eq. 3), although its contribution should be minor. As to the residue of Glu^{96}, its structure is very alike to that of Asp, as shown in Fig. 4, except that there is another $–CH_2–$ group. Therefore, the interaction mechanism of Glu and Asp is the same; that is, the Coulombic force (between $–COO^-$ and the Ca^{2+}) and the water-bridged H-bond (Fig. 6 *c*) cooperated simultaneously. The additional $–CH_2–$ lengthens the carbon chain of Glu^{96} and makes it much more flexible, so the endmost $–COO^-$ could be pulled much closer to the HAP surface. This extent will be checked by comparing the displacement of Glu^{96} (Fig. 6) and Asp^{30} (Fig. 4), where the minimal displacements are ~3 Å and ~5 Å, respectively. Correspondingly, the number of water molecules needed to form water-bridged H-bonds was one (Fig. 6 *c*) and two (Fig. 5 *c*). This also proves that the key-adsorption is much stronger than the fulcrum-adsorption. Similarly to the fulcrum-adsorption period, there is water-bridged H-bond existing between Asn^{95} and Glu^{96}, too (Fig. 6 *d*). This inter-residue water-bridged H-bond stabilizes the protein simultaneously.

In Fig. 6, the displacement between Glu^{94} and the HAP (001) surface was also shown. Although the displacement remains constant at a value of ~10 Å for a long time (also ~350 ps), there was no water-bridged H-bond between this residue and HAP during this time. Moreover, this displacement of ~10 Å is much larger than what is generally considered to form adsorption (~5 Å) (19). Noting that Glu^{94} is adjacent to Glu^{96} and Asn^{95} directly and that the time period is just the same as the adsorption time of Glu^{96} and Asn^{95}, one could judge that the Glu^{94} residue is passively pulled close to the HAP surface but it is actually not adsorbed. Now, the question is why Glu^{94} could not form adsorption with HAP while Glu^{96} could. The key factor is the orientation of $–COO^-$. Generally, the interaction is ideal if the functional groups point to the HAP (001) surface directly. At 200 ps (Fig. 2 *c*), the $–COO^-$ of Glu^{94} was perpendicular to the HAP (001) surface and deviated from it, while the $–COO^-$ of Glu^{96} was just pointing to it. The $–COO^-$ of Glu^{96} began to interact involuntarily with HAP, whereas the $–COO^-$ of Glu^{94} could not. Along with the dynamics evolution, the interaction between the Glu^{96} and HAP becomes stronger, and the displacement correspondingly smaller (Fig. 6). At ~250 ps, it has been easy for the adsorption phenomenon to be observed. During this period, the $–COO^-$ of Glu^{94} keeps vibrating, and tries to find the best site and orientation to stabilize itself. However, the thermal vibration of self-adjusting is small for each step and the orientation change needed to form interaction is large (~180°). In fact, until 400 ps, as shown in Fig. 2 *d*, the orientation of $–COO^-$ of Glu^{94} only adjusted to be parallel to the HAP (001) surface, which was still not enough to form a stable interaction. After another 200 ps self-adjusting, its orientation was pointing to the HAP (001) surface (Fig. 2 *e*); however, the key-interaction with HAP had already been broken. The whole BMP-2 began to leave the HAP surface with a relatively fast velocity. At this time, the displacement between $–COO^-$ of Glu^{94} and HAP (001) surface is still as far as 10 Å, which is too far to interact and form adsorption. To summarize, the initial relative position is important, while the initial orientation is a more effective factor to determine whether adsorption can take place or not.

Comparing the three sets of residues marked, one could find that there are three conditions for residues of proteins to be adsorbed on the HAP (001) surface. Firstly, there should be strong adsorption functional groups; for example, the $–COO^-$, which is free and not forming the peptide bond, or the –OH and $–NH_2$ groups with neighboring strongly electron-attracting groups. Secondly, the displacement should be appropriate. If the displacement were too far, the Coulombic force would decrease markedly because the force is in inverse proportion to the square of the displacement. Based on the literature (19), the protein is considered to be adsorbed if the displacement is $<\sim$5 Å. Otherwise, the number of water molecules to form a water-bridged H-bond would be no less than three, which would make the H-bond much weaker and easier to be broken. Last but not the least, the orientation of interaction residues should be appropriate. It is optimal if they point to the HAP crystallite directly, because the self-adjusting of residues via thermal vibration is random and time-consuming. The change of orientation would not be obvious for most cases. For example, it took as long as 300–400 ps for Glu^{94} to turn 90° in this system.

Concerning the interaction mechanism of adsorption between BMP-2 and HAP (001) surface, it is found that there are three types of active groups, –OH, $–NH_2$, and $–COO^-$, while only $–COO^-$ was found in many experiments for other proteins (12,13). In the case of the $–COO^-$ functional group, the forces involved in the adsorption include the Coulombic force and the water-bridged H-bond. In the case of –OH and $–NH_2$, the adsorption onto HAP surface both is through the water-bridged H-bond. To summarize, there is the Coulombic force, as stated in most literature (12,13). However, it is found that the water-bridged H-bond also plays a very important role in forming adsorption between BMP-2 and HAP crystallite. Because most residues in BMP-2 are electron-neutral, there is no Coulombic force with HAP crystallite. However, they have strong proton donor (H atom) and/or acceptor atoms (N or O atoms). Under the influence of strongly electron-attracting adjacent groups, some residues could form a water-bridged H-bond easily with HAP (001) surface through one or two water molecules. Moreover, as shown above, this type of water-bridged H-bond is strong enough to resist the external force for a relatively long time. It is the nature of interactions between residues with no net charges and HAP crystallite. It is expected that this mechanism will be helpful for the better understanding of biomineralization and for the specific applications of BMPs and HAP in tissue engineering, orthopedics, and other biological fields.

Water-bridged H-bond by quantum chemistry calculation

To obtain more accurate structural parameters for this type of water-bridged H-bond, DFT calculations were performed. The optimized structures of these water-bridged H-bonds (Figs. 5 and 6) are illustrated in Fig. 7. The data of bond lengths and angles are listed in Table 1. Here, we define the bond length of H-bond between BMP-2 and H_2O as R1 (R1′) and the angle as A1 (A1′). Correspondingly, the R2 (R2′) and A2 (A2′) mean the distance and angle of H-bond between H_2O and H_2O; for the H-bond between H_2O and HAP, they are R3 and A3.

Generally, for an H-bond of X–H–Y, the distance of H−Y is <2.45 Å, and the bond angle of X–H–Y should be >150° (i.e., <30°) (49,50). As shown in Table 1, the bond lengths optimized at the UB3LYP/6-31G* level are ≤1.952 Å, and most bond angles are >150°. As to the LDA and CHARMM27 force-field methods, the maximum *R* and the minimum *A* are 1.758 Å and 141.3°, 2.117 Å and 161.2°, respectively. All these results show that the water-bridged H-bonds do exist during the adsorption-desorption process of BMP-2 on the HAP (001) surface. Although the angles for Key-Glu[96] are <150° (A1 is 144.4° and A3 is 147.7°), the deviations are small enough to be ignored, and one could still consider this system as H-bonded. Because the Glu[96] residue is at the end part of BMP-2, the loop conformation is more readily influenced by the surrounding water molecules, which might result in this deviation from the normal criterion of H-bond. Comparing the results of the three methods we used, it is found that the CHARMM27 force field could provide correct

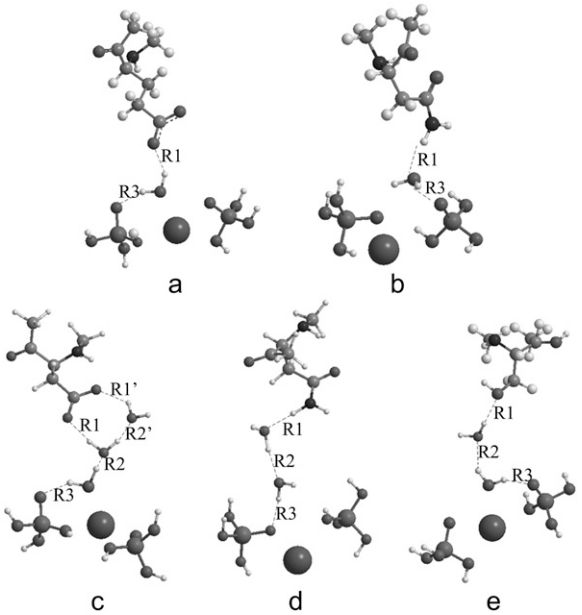

FIGURE 7 Structures of water-bridged H-bonds by quantum chemistry calculations. (*a*) Key-Glu[96], (*b*) Key-Asn[95], (*c*) Ful-Asp[30], (*d*) Ful-Asn[29], and (*e*) Ful-Ser[24]. (Atoms: Ca, *larger shaded*; P, *medium shaded*; C, *smaller light shaded*; O, *smaller shaded*; N, *smaller dark shaded*; H, *open*.)

TABLE 1 The geometric parameters of bond lengths (*R*) and bond angles (*A*) for water-bridged H-bonds using different methods (*R* in Ångstroms, and *A* in degrees)

Adsorption residues	LDA	UB3LYP/6-31G*	CHARMM27 force field
Key-Glu[96]			
R1	1.257	1.834	1.849
A1	156.2	144.4	168.3
R3	1.652	1.681	1.611
A3	143.4	147.7	171.2
Key-Asn[95]			
R1	1.799	1.762	1.968
A1	171.9	169.5	169.2
R3	1.539	1.572	1.586
A3	150.4	153.5	171.6
Ful-Ser[24]			
R1	1.366	1.952	1.935
A1	168.6	163.5	166.7
R2	1.317	1.875	1.898
A2	174.3	164.5	169.8
R3	1.689	1.648	1.598
A3	141.3	147.3	176.3
Ful-Asp[30]			
R1	1.488	1.488	1.609
A1	166.7	172.2	167.5
R1′	1.377	1.726	1.590
A1′	170.5	175.2	164.3
R2	1.154	1.573	2.117
A2	170.8	175.7	162.2
R2′	1.370	1.807	1.786
A2′	156.7	166.6	169.6
R3	1.780	1.786	1.598
A3	140.5	164.7	164.7
Ful-Asn[29]			
R1	1.758	1.756	1.868
A1	176.7	173.7	161.2
R2	1.663	1.856	1.978
A2	157.4	172.3	161.7
R3	1.713	1.733	1.712
A3	168.7	155.4	163.1

structural information qualitatively, although the data are slightly different from those obtained by DFT method.

The profile of the BMP-2 encountering the HAP should be random. Both the special texture of HAP and the special surroundings should have an influence on the adsorption-desorption behaviors of proteins on HAP. It is noticed that the interface discussed here is not sufficient for the complete study of the (BMP-2)-HAP interactions. To know more details in a systematic way, a series of simulations and atomic-force microscopy experiments have been carried out in our group. However, this adsorption-desorption process is typical and comprehensive. If there were several sets of adsorption residues on the interface of protein, like the system we discussed here, the adsorption-desorption process with HAP crystallite would most likely be stepwise. On the contrary, if there were only one set of adsorption residues, it would be much simpler and only include the last period of this process, i.e., the key-adsorption period.

CONCLUSIONS

MD, SMD simulations, and quantum chemistry calculations of the interaction between BMP-2 and HAP (001) surface were performed in an effort to understand the adsorption-desorption process for the system investigated. The results indicate that the SMD simulation could provide a good reflection of the microstructural changes for the interaction between proteins and inorganic crystals such as HAP. It could also bring some useful structural information qualitatively. The details are summarized as follows:

1. Three types of adsorption functional groups, –OH, $–NH_2$, and $–COO^-$, are found for protein BMP-2 to interact with HAP (001) surface, while most experiments for other proteins could find only one of them, i.e., the $–COO^-$ group. As active groups, they are usually neighboring with strongly electron-attracting groups directly, such as –C=O. According to the different interfaces proteins encountered with HAP crystallite, there might be one or several types of adsorption groups working simultaneously.
2. The adsorption mechanism was explored in detail. In addition to the Coulombic force, which has been widely accepted, the water-bridged H-bond is found to be very important as well. For many interactive groups, such as –OH and $–NH_2$, with no net charge, it is the water-bridged H-bond that results in the adsorption. Generally, the number of water molecules needed is not more than three. As to $–COO^-$, both Coulombic force and the water-bridged H-bond contribute to the interaction with HAP (001) surface. The results of the quantum chemistry calculations confirm that this type of water-bridged H-bond does exist.
3. The adsorption-desorption process discussed here is typical and specific. It might be alterable for different profiles of the protein. If there were several sets of adsorption groups for a certain profile, the adsorption-desorption process would most likely be stepwise. Inversely, if there were only one set, then there would be only the key-adsorption period.

The authors thank Dr. F. Huarte-Larranaga and Dr. Jin Wu for their helpful discussions.

This work was financially supported by the National Natural Science Foundation of China (grant No. 60533050 and grant No. 20503025).

REFERENCES

1. Gray, J. J. 2004. The interaction of proteins with solid surfaces. *Curr. Opin. Struct. Biol.* 14:110–115.
2. Kandori, K., A. Masunari, and T. Ishikawa. 2005. Study on adsorption mechanism of proteins onto synthetic calcium hydroxyapatites through ionic concentration measurements. *Calcif. Tissue Int.* 76:194–206.
3. Chen, X., Q. Wang, J. Shen, H. Pan, and T. Wu. 2007. Adsorption of LRAP on hydroxyapatite (001) surface through $–COO^-$ claws. *J. Phys. Chem. C.* 111:1284–1290.
4. Langer, R., and D. A. Tirrell. 2004. Designing materials for biology and medicine. *Nature.* 428:487–492.
5. Stevens, M. M., and J. H. George. 2005. Exploring and engineering the cell surface interface. *Science.* 310:1135–1138.
6. Kim, S. R., J. H. Lee, Y. T. Kim, D. H. Riu, S. J. Jung, Y. J. Lee, S. C. Chung, and Y. H. Kim. 2003. Synthesis of Si, Mg substituted hydroxyapatites and their sintering behaviors. *Biomaterials.* 24:1389–1398.
7. Matsuda, A., T. Furuzono, D. Walsh, A. Kishida, and J. Tanaka. 2003. Surface modification of a porous hydroxyapatite to promote bonded polymer coatings. *J. Mater. Sci. Mater. M.* 14:973–978.
8. Yuan, H., Z. Yang, J. D. de Bruijn, K. de Groot, and X. Zhang. 2001. Material-dependent bone induction by calcium phosphate ceramics: a 2.5-year study in dog. *Biomaterials.* 22:2617–2623.
9. Suzuki, O., S. Kamakura, T. Katagiri, M. Nakamura, B. H. Zhao, Y. Honda, and R. Kamijo. 2006. Bone formation enhanced by implanted octacalcium phosphate involving conversion into Ca-deficient hydroxyapatite. *Biomaterials.* 27:2671–2681.
10. Zahn, D., and O. Hochrein. 2005. A molecular dynamics simulation study of (OH^-) Schottky defects in hydroxyapatite. *Z. Anorg. Allg. Chem.* 631:1134–1138.
11. Zahn, D., and O. Hochrein. 2003. Computational study of interfaces between hydroxyapatite and water. *Phys. Chem. Chem. Phys.* 5:4004–4007.
12. Stayton, P. S., G. P. Drobny, W. J. Shaw, J. R. Long, and M. Gilbert. 2003. Molecular recognition at the protein-hydroxyapatite interface. *Crit. Rev. Oral Biol. M.* 14:370–376.
13. Shaw, W. J., J. R. Long, J. L. Dindot, A. A. Campbell, P. S. Stayton, and G. P. Drobny. 2000. Determination of statherin N-terminal peptide conformation on hydroxyapatite crystals. *J. Am. Chem. Soc.* 122:1709–1716.
14. Gilbert, M., W. J. Shaw, J. R. Long, K. Nelson, G. P. Drobny, C. M. Giachelli, and P. S. Stayton. 2000. Chimeric peptides of statherin and osteopontin that bind hydroxyapatite and mediate cell adhesion. *J. Biol. Chem.* 275:16213–16218.
15. Raghunathan, V., J. M. Gibson, G. Goobes, J. M. Popham, E. A. Louie, P. S. Stayton, and G. P. Drobny. 2006. Homonuclear and heteronuclear NMR studies of a statherin fragment bound to hydroxyapatite crystals. *J. Phys. Chem. B.* 110:9324–9332.
16. Wallwork, M. L., J. Kirkham, J. Zhang, S. J. Brookes, R. C. Shore, S. R. Wood, O. Ryu, C. Robinson, and D. A. Smith. 2001. Binding of matrix proteins to developing enamel crystals: an atomic force microscopy study. *Langmuir.* 17:2508–2513.
17. Bouropoulos, N., and J. Moradian-Oldak. 2003. Analysis of hydroxyapatite surface coverage by amelogenin nanospheres following the Langmuir model for protein adsorption. *Calcif. Tissue Int.* 72:599–603.
18. Becker, O. M., A. D. MacKerell Jr., B. Roux, and M. Watanabe. 2001. Computational Biochemistry and Biophysics. Marcel Dekker, New York.
19. Raffaini, G., and F. Ganazzoli. 2004. Molecular dynamics simulation of the adsorption of a fibronectin module on a graphite surface. *Langmuir.* 20:3371–3378.
20. Raffaini, G., and F. Ganazzoli. 2003. Simulation study of the interaction of some albumin subdomains with a flat graphite surface. *Langmuir.* 19:3403–3412.
21. Marszalek, P. E., H. Lu, H. Li, M. Carrion-Vazquez, A. F. Oberhauser, K. Schulten, and J. M. Fernandez. 1999. Mechanical unfolding intermediates in titin modules. *Nature.* 402:100–103.
22. Lu, H., and K. Schulten. 2000. The key event in force-induced unfolding of titin's immunoglobulin domains. *Biophys. J.* 79:51–65.
23. Isralewitz, B., J. Baudry, J. Gullingsrud, D. Kosztin, and K. Schulten. 2001. Steered molecular dynamics investigations of protein function. *J. Mol. Graph. Model.* 19:13–25.
24. Isralewitz, B., M. Gao, and K. Schulten. 2001. Steered molecular dynamics and mechanical functions of proteins. *Curr. Opin. Struct. Biol.* 11:224–230.
25. Brown, M. A., Q. Zhao, K. A. Baker, C. Naik, C. Chen, L. Pukac, M. Singh, T. Tsareva, Y. Parice, A. Mahoney, V. Roschke, I. Sanyal, and

S. Choe. 2005. Crystal structure of BMP-9 and functional interactions with pro-region and receptors. *J. Biol. Chem.* 280:25111–25118.

26. Tazaki, J., T. Akazawa, M. Murata, M. Yamamoto, Y. Tabata, R. Yoshimoto, and M. Arisue. 2006. BMP-2 dose-response and release studies in functionally graded Hap. *Key Eng. Mater.* 309–311:965–968.
27. Ono, I., T. Tateshita, M. Inoue, and Y. Kuboki. 1998. *In vivo* strength enhancement of hydroxyapatite combined with rhBMP-2. *J. Bone Miner. Metab.* 16:81–87.
28. Matsumoto, T., M. Okazaki, M. Inoue, S. Yamaguchi, T. Kusunose, T. Toyonaga, Y. Hamada, and J. Takahashi. 2004. Hydroxyapatite particles as a controlled release carrier of protein. *Biomaterials.* 25:3807–3812.
29. Duffy, D. M., and J. H. Harding. 2004. Growth of polar crystal surfaces on ionized organic substrates. *Langmuir.* 20:7637–7642.
30. Pan, H., J. Tao, T. Wu, and R. Tang. 2006. Molecular simulation of water behaviors on hydroxyapatite crystal faces. *Chinese J. Inorg. Chem.* 22:1392–1400.
31. Gonzalez-McQuire, R., J. Y. Chane-Ching, E. Vignaud, A. Lebugle, and S. Mann. 2004. Synthesis and characterization of amino acid-functionalized hydroxyapatite nanorods. *J. Mater. Chem.* 14:2277–2281.
32. Kawasaki, T., M. Niikura, S. Takahashi, and W. Kobayashi. 1986. High-performance liquid chromatography by using improved spherical hydroxyapatite particles as adsorbent: efficiency and durability of the column. *Biochem. Int.* 13:969–982.
33. Kale, L., R. Skeel, M. Bhandarkar, R. Brunner, A. Gursoy, N. Krawetz, J. Phillips, A. Shinozaki, K. Varadarajan, and K. Schulten. 1999. NAMD2: Greater scalability for parallel molecular dynamics. *J. Comput. Phys.* 151:283–312.
34. MacKerell, A. D., Jr., D. Bashford, M. Bellott, R. L. Jr. Dunbrack, J. D. Evanseck, M. J. Field, S. Fischer, J. Gao, H. Guo, S. Ha, D. Joseph-McCarthy, L. Kuchnir, K. Kuczera, F. T. K. Lau, C. Mattos, S. Michnick, T. Ngo, D. T. Nguyen, B. Prodhom, W. E. I. I. I. Reiher, B. Roux, M. Schlenkrich, J. C. Smith, R. Stote, J. Straub, M. Watanabe, J. Wiorkiewicz-Kuczera, D. Yin, and M. Karplus. 1998. All-atom empirical potential for molecular modeling and dynamics studies of proteins. *J. Phys. Chem. B.* 102:3586–3616.
35. Hauptmann, S., H. Dufner, J. Brickmann, S. M. Kast, and R. S. Berry. 2003. Potential energy function for apatites. *Phys. Chem. Chem. Phys.* 5:635–639.
36. Hirschfelder, J. O., C. F. Curtiss, and R. B. Brid. 1954. Molecular Theory of Gases and Liquids. John Wiley and Sons, New York.
37. Harding, J. H., and D. M. Duffy. 2006. The challenge of biominerals to simulations. *J. Mater. Chem.* 16:1105–1112.
38. Gao, H., and Y. Kong. 2004. Simulation of DNA-nanotube interactions. *Annu. Rev. Mater. Res.* 34:123–150.
39. Ravichandran, S., J. D. Madura, and J. Talbot. 2001. A Brownian dynamics study of the initial stages of hen egg-white lysozyme adsorption at a solid interface. *J. Phys. Chem. B.* 105:3610–3613.
40. Berendsen, H. J. C., J. P. M. Postma, W. F. van Gunsteren, and J. Hermans. 1981. Intermolecular models for water in relation to protein hydration. *In* Intermolecular Forces. B. Pullman, editor. Reidel, Dordrecht, The Netherlands.
41. Darden, T. A., D. M. York, and L. G. Pedersen. 1993. Particle mesh Ewald: an $N\cdot\log(N)$ method for Ewald sums in large systems. *J. Chem. Phys.* 98:10089–10092.
42. Delley, B. 1990. An all-electron numerical method for solving the local density functional for polyatomic molecules. *J. Chem. Phys.* 92: 508–517.
43. Delley, B. 2000. From molecules to solids with the $DMol^3$ approach. *J. Chem. Phys.* 113:7756–7764.
44. Frisch, M. J., G. W. Trucks, H. B. Schlegel, G. E. Scuseria, M. A. Robb, J. R. Cheeseman, J. A. Montgomery, Jr., T. Vreven, K. N. Kudin, J. C. Burant, J. M. Millam, S. S. Iyengar, J. Tomasi, V. Barone, B. Mennucci, M. Cossi, G. Scalmani, N. Rega, G. A. Petersson, H. Nakatsuji, M. Hada, M. Ehara, K. Toyota, R. Fukuda, J. Hasegawa, M. Ishida, T. Nakajima, Y. Honda, O. Kitao, H. Nakai, M. Klene, X. Li, J. E. Knox, H. P. Hratchian, J. B. Cross, C. Adamo, J. Jaramillo, R. Gomperts, R. E. Stratmann, O. Yazyev, A. J. Austin, R. Cammi, C. Pomelli, J. W. Ochterski, P. Y. Ayala, K. Morokuma, G. A. Voth, P. Salvador, J. J. Dannenberg, V. G. Zakrzewski, S. Dapprich, A. D. Daniels, M. C. Strain, O. Farkas, D. K. Malick, A. D. Rabuck, K. Raghavachari, J. B. Foresman, J. V. Ortiz, Q. Cui, A. G. Baboul, S. Clifford, J. Cioslowski, B. B. Stefanov, G. Liu, A. Liashenko, P. Piskorz, I. Komaromi, R. L. Martin, D. J. Fox, T. Keith, M. A. Al-Laham, C. Y. Peng, A. Nanayakkara, M. Challacombe, P. M. W. Gill, B. Johnson, W. Chen, M. W. Wong, C. Gonzalez, and J. A. Pople. 2003. Gaussian 03, Rev. B.02. Gaussian, Pittsburgh, PA.
45. Kakkar, R., P. N. Kapoor, and K. J. Klabunde. 2006. First principles density functional study of the adsorption and dissociation of carbonyl compounds on magnesium oxide nanosurfaces. *J. Phys. Chem. B.* 110: 25941–25949.
46. Toth, R., M. Ferrone, S. Miertus, E. Chiellini, M. Fermeglia, and S. Prici. 2006. Structure and energetics of biocompatible polymer nanocomposite systems: a molecular dynamics study. *Biomacromolecules.* 7:1714–1719.
47. Yoshizawa, K., and Y. Shiota. 2006. Conversion of methane to methanol at the mononuclear and dinuclear copper sites of particulate methane monooxygenase (pMMO): a DFT and QM/MM study. *J. Am. Chem. Soc.* 128:9873–9881.
48. Scheiner, S., and T. Kar. 2005. Effect of solvent upon CH···O hydrogen bonds with implications for protein folding. *J. Phys. Chem. B.* 109:3681–3689.
49. Jorgensen, W. L. 1980. Quantum and statistical mechanical studies of liquids. 7. Structure and properties of liquid methanol. *J. Am. Chem. Soc.* 102:543–549.
50. Jorgensen, W. L., and M. Ibrahim. 1982. Quantum and statistical mechanical studies of liquids. 20. Pressure dependence of hydrogen bonding in liquid methanol. *J. Am. Chem. Soc.* 104:373–378.